Thermodynamic and kinetic properties of hot nonideal plasmas

To cite this article: W Ebeling *et al* 1996 *Plasma Phys. Control. Fusion* **38** A31

Plasma Phys. Control. Fusion **38** (1996) A31–A47. Printed in the UK

Thermodynamic and kinetic properties of hot nonideal plasmas

W Ebeling†, A Förster†, H Hess‡ and M Yu Romanovsky†§

† Institute of Physics, Humboldt University Berlin, Germany

‡ Institute of Low-Temperature Plasma Physics, Greifswald, Germany

§ General Physics Institute, Academy of Science, Moscow, Russia

Abstract. A survey of theoretical and experimental results on plasmas with strong Coulomb interactions is given. First the basic theoretical concepts describing nonideality, degeneracy and screening are introduced. The general structure of the thermodynamic functions and the phase diagram in the density–temperature plane is explained. Relevant experiments including shock waves and pulse-produced plasmas are briefly reviewed. Results on the critical data, thermodynamic and electric properties around the critical point and in supercritical states are discussed. The existence of high-pressure, high-temperature plasma phase transitions is investigated. After a brief discussion of transport properties the kinetics of ionization and reaction processes is studied. The influence of nonideality on ionization and nuclear fusion rates is investigated.

1. Introduction

More than 90% of matter in the universe and, especially, the stars and the giant planets are in the state of dense plasmas. In many of these plasmas the mean potential energy is of the same order of magnitude as the mean kinetic energy. Then we speak about nonideal plasmas, or sometimes the term strongly coupled plasmas is used. The physical properties of such plasmas are determined by the Coulomb interaction between the charged plasma particles. Dense plasmas play an important role in nature, laboratory experiments and in technology. Correct understanding of the structure and evolution of the most interesting astrophysical objects such as the Sun, the giant planets, white and brown dwarfs, is impossible without the consideration of Coulomb effects. The plasmas in alternative fusion concepts based on pellet compression with laser and heavy-ion beams cross the region of strong coupling. Ordinary devices like high-pressure discharge lamps used on streets or vacuum-arc cathode spots which appear in tokamaks as well as in high-current vacuum interrupters involve dense plasmas. These and other examples are shown in figures 1 and 2. Dense nonideal plasmas are a difficult, but rather interesting field of modern research [1–4]. Such plasmas also play a major role in modern technologies. For example, high-energy pulse power technology is at least partially based on the generation and application of strongly coupled plasmas because the high energy density connected with this technology requires high particle densities in the carrier material and also a practically indestructible medium with a short recovery time after load.

The consequent theoretical treatment of dense plasmas demands quantum statistics of interacting many-particle systems. The most important physical effects of the Coulomb interaction and of the quantum-mechanical uncertainty and exchange are: lowering the border between the discrete and the continuous energy spectrum, thus lowering

0741-3335/96/SA0031+17$19.50

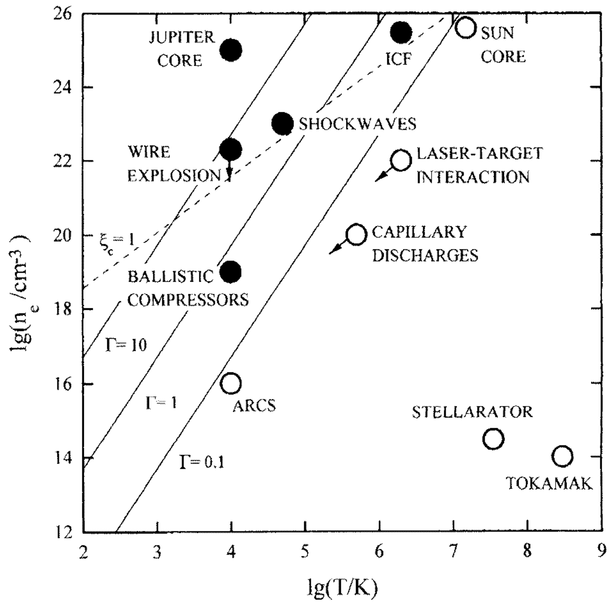

Figure 1. The location of several plasmas from nature, laboratory experiment and technology in the electron-density–temperature plane. Above the dashed line the electrons in the plasma are degenerate. The lines $\Gamma = 0.1, 1.0, 10$ mark the border between ideal and strongly coupled plasmas.

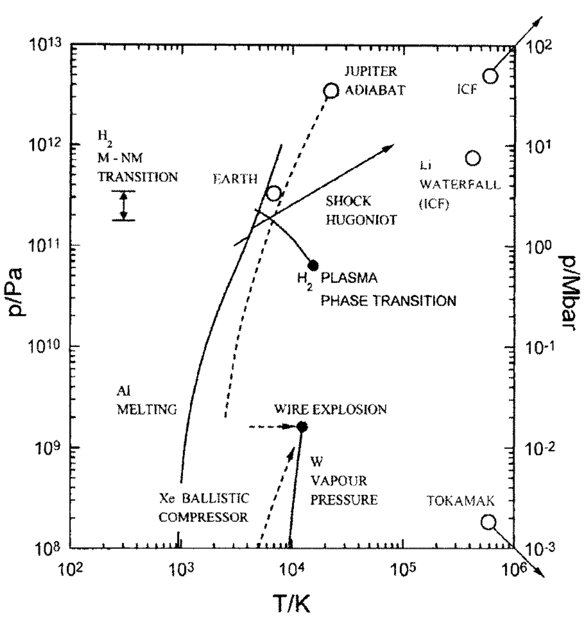

Figure 2. The location of several plasmas in the pressure–temperature plane. Below we show additionally the coexistence line and the critical point for the liquid–gas transition in tungsten. In the centre of the diagram a theoretical result for the coexistence line and the critical point of the plasma phase transition in hydrogen is shown. At lower temperatures it corresponds to the metal–nonmetal (M–NM) transition in solid molecular hydrogen.

the effective ionization and excitation energies, shift and broadening of spectral lines, exponential enhancement of excitation processes as well as fusion rates, modifications of the equation of state, pressure ionization and the appearance of new high-pressure phase transitions.

The structure of this review is as follows. In section 2 we introduce some dimensionless plasma parameters, outline an elementary theory for the thermodynamic functions, summarize experimental as well as theoretical results for thermodynamics and phase transitions. Section 3 is devoted to kinetic processes and, in particular, to reaction kinetics for electronic and fusion processes. The kinetic equations are given and the nonideal reaction rates are derived.

2. Thermodynamic properties

2.1. Theoretical plasma thermodynamics

The thermodynamics of nonideal plasmas is quite different from the thermodynamics of real gases; this is mainly due to the long-range character of the Coulomb potential [6]. For one-component plasmas consisting of one type of ions and a neutralizing uniform background the characteristic parameter of nonideality is

$$\Gamma = (e^2/k_B T d_i) \tag{1}$$

where d_i is the average distance of the ions defined by

$$(4\pi/3)d_i^3 = V/N_i = n_i^{-1}. \tag{2}$$

Here n_i is the ion density and k_B is Boltzmann's constant. In the classical case the interaction part of the free energy per particle (in units of $k_B T$) depends only on Γ. Quantum effects lead to important corrections to the classical behaviour; in particular we mention the existence of bound states and symmetry effects [1, 5]. Recently, the theory of quantum plasmas succeeded in making considerable progress in the calculation of thermodynamic functions [7, 9–12, 15]. As is well known, modern theory of quantum plasmas uses a whole spectrum of methods such as the approach based on Slater sums [7, 11], the Green's function technique [1, 11], the density functional technique [9], quantum Monte Carlo methods [17, 18], wavepacket dynamics [19, 20] and other methods [2, 13, 14, 22]. Several new results were obtained recently with the help of an approach based on the Feynman–Kac technique [15]. In general, each of these methods is particularly useful for calculations in specific parts of the density–temperature plane or for solving special problems. For example, the technique of Slater sums in combination with cluster expansions is well suited for the low-density region [7, 8]. The Green's function method and the density functional method are more appropriate for the degenerate region [1, 9, 11].

Using the method of Slater sums in 1968–70 the density expansions of the pressure and the free energy density were studied systematically. In this way exact expressions for the contributions of the orders $O(n^{3/2})$, $O(n^2 \log n)$ and $O(n^2)$ were calculated without any approximations [1, 7]. Further, the order $O(n^{5/2})$ was calculated approximately [11, 16]. New calculations by means of the Feynman–Kac technique and by the Green's function technique reconfirmed these expressions and gave a new result for the contribution of the order $O(n^{5/2})$ [15, 21]. In some sense the statistical thermodynamics of plasmas has followed a similar path to the theory of real gases about a quarter of a century earlier, where the theory started with virial expansions and arrived more and more at closed expressions [2, 5]. Therefore considerable effort was devoted to the calculation of higher-order contributions to the EOS and other thermodynamic functions. The significance of exact expressions for the higher-order terms in virial expansions is, in particular, connected with the existence of new, very precise measurements for the EOS based on astrophysical observations [28]. Further, we also mention the new rather precise shock compression experiments [29, 51]. One may hope that in the near future new expressions for the higher-order quantum corrections up to order $O(n^3)$ will be available. This would allow us to include the three-particle quantum effects. A strong argument in favour of these efforts is:

(i) long experience of workers in the theory of real (neutral) gases has shown that the calculation of higher-order virial coefficients gives a lot of insight into the structure of the full thermodynamic functions and

(ii) the knowledge of higher-order terms provides good possibilities for constructing Padé approximations [2, 12, 24, 26, 27].

Let us now consider a simple version of the thermodynamic theory, the so-called Lambda approximation [1, 2, 14, 22, 23]. This approach is closely related to the Debye–Hückel theory for classical charged hard spheres with a fixed diameter a. In the Lambda approximation we use the same analytical form as the Debye–Hückel theory, but with a temperature-dependent quantum length $a(T)$ instead of the classical parameter a. In addition to the Debye–Hückel terms, van der Waals terms are also introduced into the thermodynamic functions. One can easily show by using Heisenberg's uncertainty relation that a reasonable choice of the quantum diameter is given by the thermal de Broglie wavelength

$$a(T) = \Lambda/8 \tag{3}$$

$$\Lambda = h/(2\pi m_e k_B T)^{1/2}. \tag{4}$$

In a recent analysis it was shown that the simple analytical structure of the Lambda approximation yields, at least semi-quantitatively, a correct behaviour in the density–temperature plane, even including phase transitions [1, 14, 22]. Therefore one can recommend this simple approximation for a first analysis of the thermodynamic properties of quantum plasmas. This approximation is, however, restricted to nondegenerate plasmas. The Debye–Hückel formulae for the thermodynamic functions in the Lambda approximation are to be completed by a Saha equation. We consider only the simplest case $Z = 1$, and introduce the total number density of heavy particles $n = n_0 + n_i = n_0 + n_e$. The degree of ionization is defined by $\gamma = n_i/n = n_e/n$. Now the Saha equation reads

$$\frac{1-\gamma}{\gamma^2} = n_a \Lambda^3 \sigma(T) \exp\left(-\frac{\Delta I}{k_B T}\right). \tag{5}$$

Here

$$\Delta I = \frac{e^2 \kappa \sqrt{\gamma}}{k_B T (1 + \kappa a(T)\sqrt{\gamma})} - W n(2\gamma - 1) \tag{6}$$

is the lowering of the ionization energy. Further, W denotes the coefficient of a polarization contribution which is of particular importance for alkali plasmas and for mercury plasmas [31].

Let us now briefly discuss a more complicated approach named PACH, which means Padé approximation in the chemical picture [2, 27]. Padé approximations of the interaction contributions of thermodynamic functions [2] are based on an interpolation between the analytical expressions at low densities (virial expansions) and the known limits at very high densities. The simple analytical form of the Padé formulae allows fast access to different thermodynamic properties over a wide range of density and temperature. The free energy of the plasma is represented in a similar form to the Lambda approximation but with more complicated functions for the Coulomb and for the van der Waals contributions. In order to find the thermodynamic equilibrium within the Padé approximation in the chemical picture (PACH) for a given temperature and density one has to minimize the free energy with respect to the abundancies of the various free and composite particles [30]. After performing this procedure on a dense grid in the density–temperature plane one can calculate different thermodynamic properties.

In recent work [27, 30] we have calculated, within the PACH approach, the pressure factor $p/p_{\mathrm{id}}^{\mathrm{F}}$, where p is the actual pressure and $p_{\mathrm{id}}^{\mathrm{F}}$ denotes the ideal pressure of a fully ionized plasma derived from Fermi–Dirac statistics. In figure 3 we compare our PACH results at a fixed density with recent path-integral Monte Carlo simulations from Pierleoni *et al* [18], we find a reasonable agreement. In figure 4 the lines of constant pressure factor in the density–temperature plane taken from [27] are represented for H plasmas. We see that the nonideality region with respect to the pressure is located in the left-hand lower corner of the density–temperature plane (the so-called corner of correlations).

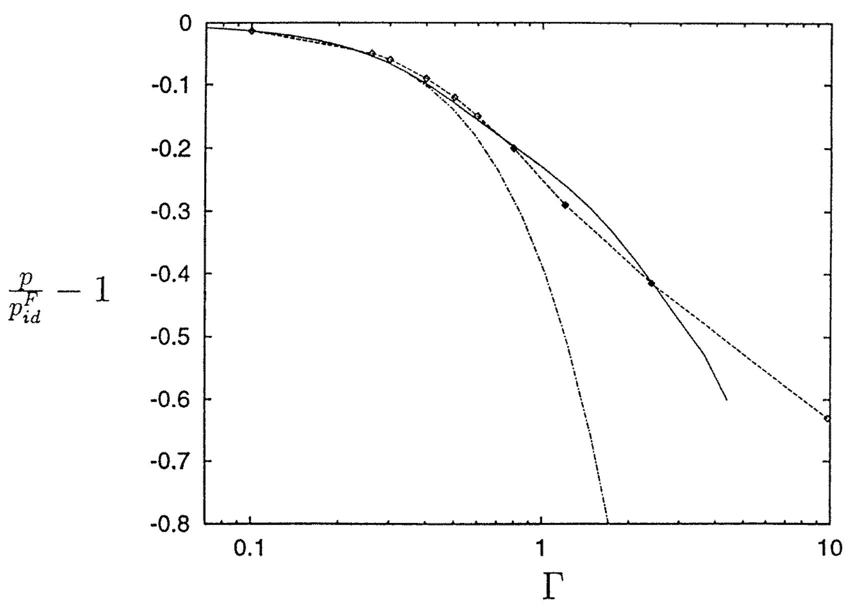

Figure 3. The pressure factor over the coupling parameter Γ for three different approaches: ionization equilibrium within the Padé approximations in the chemical picture, PACH (full curve), path-integral Monte Carlo simulations by Pierleoni *et al* (broken curve), ionization equilibrium in the Debye model (dashed-dotted curve).

2.2. *Phase transitions and experimental investigations*

As is well known, real gases with attractive interactions show a first-order phase transition described in the p–T plane by a critical point C_1 and a coexistence line ending at C_1. Assuming that in our expressions for the free energy the Coulombic terms are omitted, a simple van der Waals type expression is obtained with the critical point

$$T_{C_1} = \frac{8A}{27k_B B} \qquad n_{C_1} = \frac{1}{3B}. \tag{7}$$

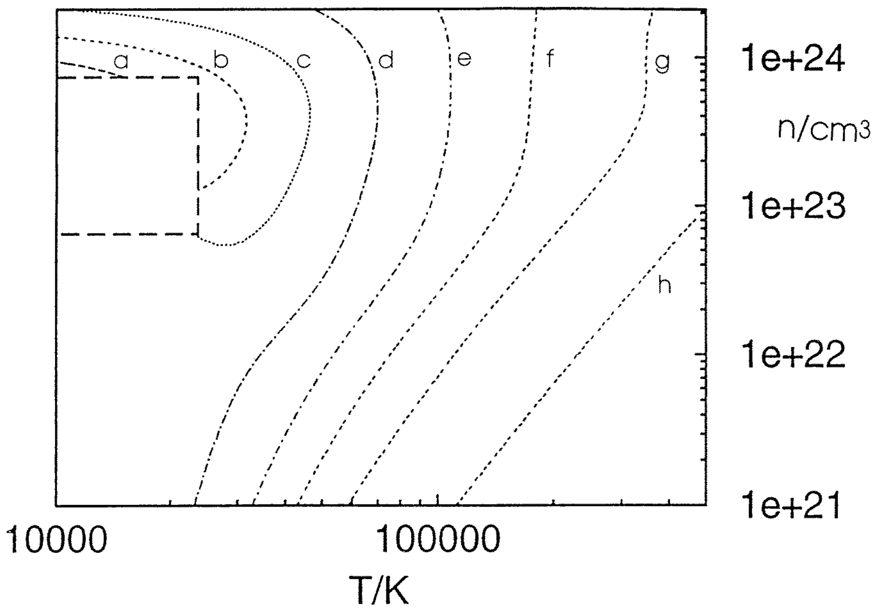

Figure 4. Lines of constant pressure factor for a hydrogen plasma calculated with PACH. The values of the pressure factor $p/p_{\mathrm{id}}^{\mathrm{F}}$ are: (*a*) 0.25, (*b*) 0.35, (*c*) 0.45, (*d*) 0.55, (*e*) 0.65, (*f*) 0.75, (*g*) 0.85, (*h*) 0.95.

It is well known that in systems with a long-range Coulomb interaction, besides the classical first-order phase transition typical for neutral gases, a second first-order phase transition may appear. In the coexistence region of this transition the system is divided into two phases of different degrees of ionization and different mass density. This is the so-called plasma phase transition (PPT). The existence of a phase diagram including a separate PPT was discussed for the first time in 1943 by Landau and Zeldovich [32]. First calculations of the plasma phase transition are due to Norman and Starostin [33], Ebeling and co-workers [1, 34]. In spite of the quantitative corrections with regard to the exact location of the critical points and the coexistence line [2, 4, 36] there are several statements which are independent of the nature of the approximations:

(i) In the p–T diagram, the pressure region beyond one gigapascal includes a line of a first-order phase transition connected with delocalization of electrons. This is the metal–nonmetal transition or Mott transition [1, 37, 38].

(ii) At lower temperatures this transition corresponds to a dielectric–metal transition whereas at higher temperatures ($T > 10^3$ K) the plasma phase transition occurs.

(iii) Above the critical temperature T_{C_2} instead of a sharp transition, a soft transition to full ionization is observed with increasing pressure.

Omitting the van der Waals and the polarization contributions in the Lambda approximation, the critical point of the PPT may be obtained analytically [1, 14, 22]. We find the critical temperature

$$T_{C_2} = \frac{e^2}{8k_B a_B} \simeq 13\,000 \text{ K} \tag{8}$$

and the critical density of the free electrons (a_B is the Bohr radius)

$$n_{C_2} = a_B^{-3} \simeq 2.7 \times 10^{20} \text{ cm}^{-3}. \tag{9}$$

In the general case that all interactions are simultaneously present, investigation of the critical conditions requires numerical methods. However, under conditions where $T_{C_1} \ll T_{C_2}, n_{C_1} \ll n_{C_2}$ the estimates given by (8) and (9) remain valid, at least approximately. In real systems this case would correspond to hydrogen [34, 36], helium [14, 24] and to noble gas plasmas [25]. Recently, the model case of symmetrical plasmas was studied by Lehmann and Ebeling [22]. This case may be of some interest for applications to electron–hole plasmas in semiconductors or possibly in the future to electron–positron plasmas.

In metallic plasmas (such as Cs, Na, K, Rb, Hg) the existence of one first-order phase transition is a well known fact [39, 43]. There is much experimental and theoretical evidence that this phase transition in metals is due to a fusing of the van der Waals transition and the plasma phase transition. We therefore find in metals a transition which is a mixture of both types. In the simple model given by the Lambda approximation the case of metals would correspond to the conditions

$$T_{C_1} \simeq T_{C_2} \qquad n_{C_1} \simeq n_{C_2}. \tag{10}$$

In metals the thermodynamic properties in the region of the unified phase transition are determined by van der Waals interactions and by Coulomb interactions. This leads to a rather complicated behaviour around the critical point [39, 42].

Let us now consider the situation for hydrogen plasmas in more detail. Figure 5 shows the estimated p–T diagram of hydrogen. In the upper right-hand corner different lines of coexistence and critical points of the PPT calculated by different authors are also shown [34, 36] and further data points from shock-wave experiments in hydrogen (H) and deuterium (D) are shown [50, 51]. With respect to the coexistence line we note that the slope $\mathrm{d}p/\mathrm{d}T$ is negative, as a consequence of the effects of pressure ionization and temperature ionization. As temperature increases the predicted transition pressure is about one order of magnitude lower than the low-temperature transition pressure for the nonmetal–metal transition. This can be understood in the light of rather crude approximations. For high temperatures the Lambda approximation may be used to describe the behaviour of partially ionized plasmas. At lower temperatures, coexistence between a molecular dielectric and a metallic liquid is expected. The condition for this transition was estimated by Marley and Hubbard (MH) [38]. Earlier shock-wave experiments in hydrogen and deuterium [50] pass the region of interest without showing signs for such a phase transition (figure 5). These experiments were characterized by calculating the density and the pressure from shock velocity and the temperature from a model EOS. Typically, such experiments supply some isolated points in a state diagram rather than continuous curves. Further, the EOS used in the analysis of the experiment was not the same as that used in the theoretical predictions. Therefore the conclusions drawn by these authors about the nonexistence of the described plasma phase transition were not convincing. Recently, the same group from Los Alamos [51] has measured electrical conductivity produced by shock waves in the relevant region. A nonmetal–metal transition has been found; however, not as a sudden jump but as a transition over a certain range of temperature (2200–3000 K) and pressure (90–140 GPa). Again the authors' denial of the whole plasma phase transition on the basis of only these results does not seem convincing. In fact, a transition to a highly ionized state was observed and it seems to be too early to draw conclusions about the exact nature of this transition. Moreover, the experimental result should be discussed critically and attract more theoretical work on this low-temperature part of the phase transition. The point of view of the present authors is that the low-temperature nonmetal–metal transition and the high-temperature PPT are

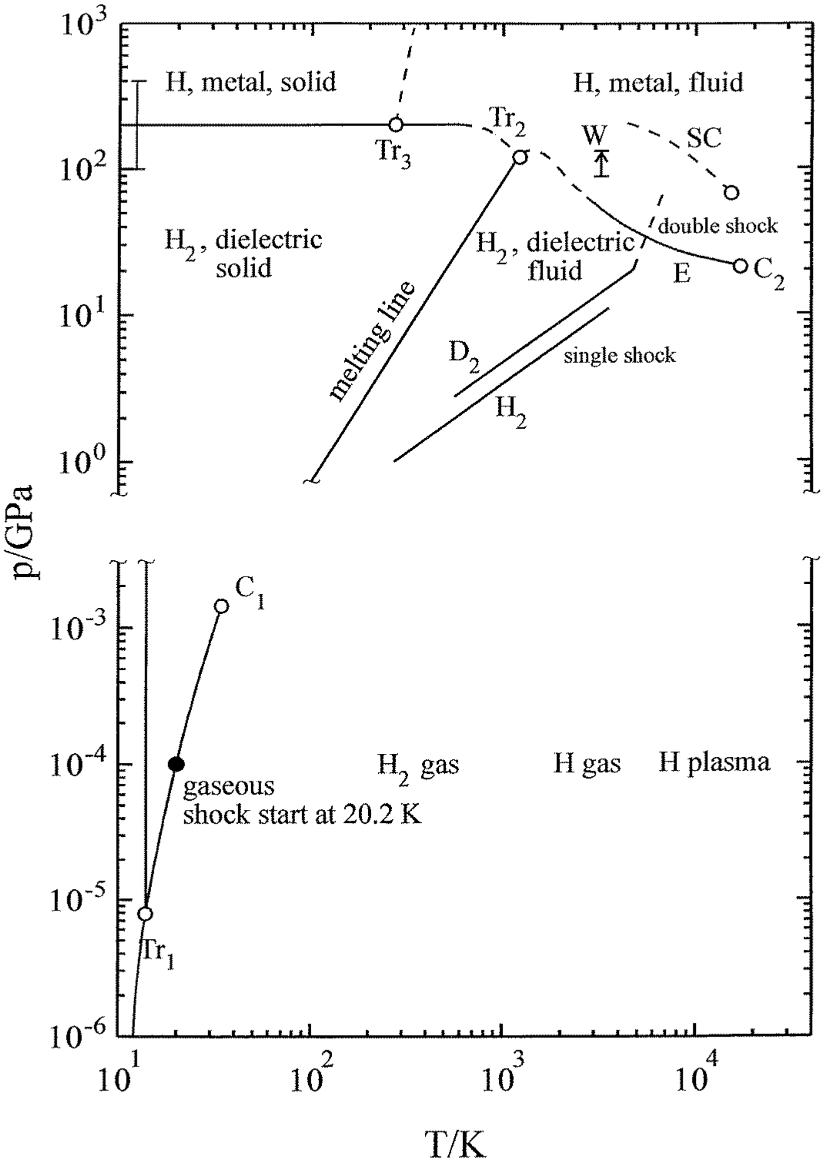

Figure 5. Phase diagram of hydrogen in the pressure–temperature plane. The notations are: C_1, critical point of the liquid–gas transition; C_2, critical point of the plasma phase transition; Tr_1, triple-point dielectric solid/dielectric liquid/dielectric gas; Tr_2, triple-point dielectric solid/dielectric fluid/metallic fluid (dense fully ionized plasma); Tr_3, triple-point dielectric solid/metallic fluid/metallic solid. The dotted curve corresponds to shock-wave data in hydrogen (H) and deuterium (D). W is the metallization area according to Weir *et al* (1996).

just two sides of the same thing. We also mention new static high-pressure experiments in the megabar region resulting in detailed analysis of the phase diagram of deuterium plasmas at low temperatures [52]. The reason for the existence of two phase transitions in hydrogen and in noble gases can be found in the large differences between the energies of dissociation and ionization of these gases (about three orders of magnitude). In metals, however, the metal–nonmetal transition is closely related to the liquid–gas transition. Here, both energies differ by less than one order of magnitude. Using an equation of state for the environment of the critical point in a metallic fluid derived by Likhalter [42] on the basis of percolation theory, critical data [43] and data on the metal–nonmetal transition have been obtained.

3. Kinetic and transport properties

3.1. Transport properties and rate equations

Dense plasmas are collision-dominated; therefore, the laws of irreversible thermodynamics hold, as a rule, to a very good approximation. There has been a lot of theoretical as well as experimental work devoted to transport coefficients of dense plasmas. As a survey we mention several monographs and original papers [2, 29, 31, 49, 54].

The overwhelming majority of theoretical work is focused on the electrical conductivity which is mainly determined by the mobility of the electrons. If the effective collision frequency is given by ν_e then the conductance will be given by

$$\sigma = n_e e^2/(m_e \nu_e). \tag{11}$$

The problem now is to calculate the collision frequency which is strongly influenced by Coulomb effects (see e.g. [49]). Of particular interest for theoretical and practical reasons is the conductivity of metallic plasmas around the critical point. In an expanding metal, the electrical conductivity decreases with decreasing density. To some extent, temperature does not influence the conductivity essentially. During the expansion process, the critical density will be passed more or less below or above the critical point depending upon the pressure reached. At this point, the conductivity of the alkali metals rubidium and caesium [40] remains well above the so-called minimum metallic conductivity [37] of about 200 Ω^{-1} cm^{-1}, which means that the vapour—not too far from the critical point—shows metallic conductivity, or, in other words, the metal–nonmetal transition does not occur until the critical density has been passed (i.e. at lower than critical density). It is expected (but experimentally not yet verified) that most other metals behave in a similar way. Mercury, however, shows quite different behaviour. During the expansion of mercury by heating, there is a remarkable change in its electrical properties before the critical density has been reached, i.e. at higher than the critical density [39]. At the critical point, the electrical conductivity is as low as about 1 Ω^{-1} cm^{-1}. Mercury is no longer a metal; the metal–nonmetal transition occurs at higher than the critical density. Mindful of these circumstances, Young [41] expressed his conviction that '. . . the metal–nonmetal transition and its connection with the liquid–vapour transition is a major challenge both experimentally and theoretically. Given the experience so far with mercury, it would not be surprising if new exotic states of matter occurred in hot, expanded metals which are presently inaccessible to experimental work'. The conductivity of the following elements should show mercury-like behaviour: the alkaline-earth metal magnesium but not beryllium, strontium and barium (no data for calcium are available), the metals of the IIB group zinc, cadmium and, of course, mercury itself, the semi-metals arsenic and antimony (VA; no data are available for bismuth), and finally selenium and tellurium of the VIA group. For selenium, there already exists an experimental hint about very low electrical conductivity at its critical point [44]. The electrical conductivity of tungsten is similar to that of copper [45, 46] at the critical point higher than 10^3 Ω^{-1} cm^{-1}, and it therefore has metallic character. For zinc, however, there is a prediction based on a theory of Likhalter [42] that the metal–nonmetal transition will occur at $\rho/\rho_c = 1.39$. As can be seen from figure 6 zinc has, at the corresponding reduced density, a metallic conductivity comparable to that of tungsten ($\simeq 3 \times 10^3\ \Omega^{-1}\ \mathrm{cm}^{-1}$). Although the conductivity of zinc afterwards decreases much faster than that of tungsten with increasing expansion, it reaches the metal–nonmetal transition (the minimum electrical conductivity) only at $\rho/\rho_c = 0.5$ and not at 1.39 as predicted.

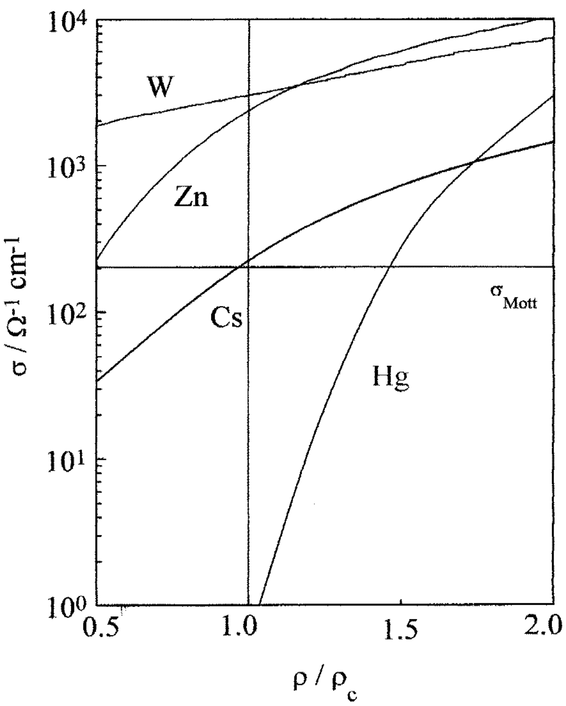

Figure 6. Conductivities of tungsten, zinc, caesium and mercury over the reduced mass density. In this density region the conductivities depend only weakly on the temperature. The horizontal line marks the Mott conductivity.

Recently, new experimental findings of a conductivity increase over more than three orders of magnitude in hydrogen between 93 and 140 GPa and corresponding temperatures between 2200 and 3000 K were reported [51]. Whether these results are already sufficient for the conclusion 'that the first-order phase transition predicted to occur at 100 GPa and 10 000 K between weakly dissociated and substantially dissociated fluid phases probably does not occur', is so far not convincing.

In contrast, this experiment is located just in the low-temperature range of the predicted plasma phase transition between the results of Ebeling and Richert (lower values) and Saumon and Chabrier (higher values), and it is (as we see it) a strong support for the metal–nonmetal transition which may be modified at lower temperatures by dissociation.

Let us now consider the kinetics of ionization processes. We will assume that the plasma is thermalized, i.e. the electron and ion velocities are distributed according to a Maxwellian distribution and that the electron temperature is equal to the ion temperature. In general this is not exactly true, but dense plasmas are in most cases isothermal, which is due to the strong coupling between the electrons and the ions. We further assume that all electrons in bound states are in thermal equilibrium. In order to describe ionization processes we have to include impact ionization and three-body recombination:

$$\mathrm{a} + \mathrm{e} \rightarrow \mathrm{i} + \mathrm{e} + \mathrm{e} \qquad \mathrm{i} + \mathrm{e} + \mathrm{e} \rightarrow \mathrm{a} + \mathrm{e}. \tag{12}$$

Here the abbreviations a, i, e denote as above the atomic, ionic and electronic species, respectively. The kinetic equations describing the ionization process read [2]

$$\dot{n}_0 = -\alpha n_\mathrm{e} n_0 + \beta n_\mathrm{e}^2 n_\mathrm{i} \tag{13}$$

where α is the ionization coefficient and β the recombination coefficient. The influence of nonideality on these coefficients will be discussed later.

Ionization processes in multiply charged plasmas and internal electron transitions which have a large influence on many properties of plasmas may be treated in a similar way [2, 27, 53, 56–58]. We mention here only first attempts to simulate ionization processes in hydrogen by new methods of quantum molecular dynamics [20].

Finally, let us consider a fusion reaction

$$\mathrm{d} + \mathrm{p} \rightarrow \mathrm{He} \tag{14}$$

occurring in a dense plasma. The rate equations will assume the form

$$\dot{n}_\mathrm{He} = R n_\mathrm{p} n_\mathrm{d} - S n_\mathrm{He} \tag{15}$$

where R is the fusion rate coefficient and S the decay (fission) coefficient. The influence of nonideality on these coefficients will be discussed in the next section.

3.2. Nonideality effects in reaction rates

Let us first consider the rate coefficients in ideal plasmas. In this limiting case the rate coefficients for ionization or excitation of an atom or ion are obtained by averaging a cross section $\sigma(v)$ over the Maxwell velocity distribution. The cross sections are available from quantum mechanical calculations and from measurements [54]. For practical calculations several interpolation formulae are available [20]. Let us now study the influence of nonideality on the rates. The rate equations for the ionization reaction yield, in the equilibrium case,

$$\alpha n_\mathrm{e} n_0 = \beta n_\mathrm{e}^2 n_\mathrm{i}. \tag{16}$$

The condition that this is consistent with the nonideal Saha equation gives

$$\frac{\beta}{\alpha} = \Lambda^3 \sigma(T) \exp\left(-\frac{\Delta I}{k_\mathrm{B} T}\right). \tag{17}$$

Taking into account the ideal case we finally get the condition

$$\frac{\alpha}{\beta} = \frac{\alpha_\mathrm{id}}{\beta_\mathrm{id}} \exp\left(\frac{\Delta I}{k_\mathrm{B} T}\right). \tag{18}$$

In other words, the relation between the ionization and the recombination coefficients is given by a purely thermodynamic quantity, the lowering of the ionization energy, which strongly increases with the density. From these considerations we can just find the corrections to the relations of rates. In order to find the individual rates we need an additional assumption. In a dense nonideal plasma it can be shown that the recombination coefficients depend only weakly on the nonideality [2, 53, 59]. Therefore the rate coefficients are given approximately by

$$\beta = \beta_\mathrm{id} \qquad \alpha = \alpha_\mathrm{id} \exp\left(\frac{\Delta I}{k_\mathrm{B} T}\right). \tag{19}$$

Here $\Delta I > 0$ is the decrease in ionization energy which in the Lambda approximation is given by (6). This assumption is in agreement with quantum-statistical results of Klimontovich [53] and other workers [2, 56, 57]. In a similar way one can treat the more complicated case where transitions between different ionic charges and excitation processes are included [54, 58]. We mention here only several interesting applications of these equations to plasmas of practical interest such as, for example, carbon and polyethylene plasmas [58].

Finally, let us study the influence of nonideality on the rates of fusion reactions. The rate equations for the fusion reaction yield, in the equilibrium case,

$$R n_{\mathrm{p}} n_{\mathrm{d}} = S n_{\mathrm{He}} \,. \tag{20}$$

The condition that this is consistent with the nonideal mass action law yields, in a similar way as shown above in the Lambda approximation,

$$\frac{R}{R_{\mathrm{id}}} = \frac{S}{S_{\mathrm{id}}} \exp\left(\frac{e^2\kappa}{k_{\mathrm{B}}T(1+\kappa a(T))}\right). \tag{21}$$

In other words, the relation between the fusion rate and the decay rate is again given by a purely thermodynamic quantity. From these considerations we can just find the corrections to the relations of rates. In order to find the individual rates we need an additional assumption. According to the investigations of several researchers [60, 61] the nonideality influences mainly the fusion rates, and leaves the decay rates unchanged. In other words we get in some approximation the enhancement rate

$$A = \frac{R}{R_{\mathrm{id}}} = \exp\left(\frac{e^2\kappa^*}{k_{\mathrm{B}}T(1+\kappa a(T))}\right). \tag{22}$$

Several even more general expressions of this type were derived by studying the pair distribution nucleus–nucleus at small distances [60, 61]. According to Ichimaru [61] the enhancement factor for fusion processes inside the Sun is estimated as $A \simeq 1.02$ according to a nonideality factor $\Gamma \simeq 0.04$. For the case of inertial confinement fusion Ichimaru estimates $A \simeq 1.01$ according to $\Gamma \simeq 0.01$. For the (so far hypothetical) case of low-temperature fusion in solid metal deuterides Ichimaru obtains very high enhancement rates $\log_{10} A \simeq 5$–10 [61].

Microscopic calculations of the fusion reaction of two nuclei have been done already by Gamov. Taking into account the Boltzmann distribution of particle energy, heat rates of thermonuclear syntheses were later obtained by Thompson [63]. There were many attempts to improve Gamov's theory by accounting for the influence of surrounding particles on two-body nuclear reactions. Previously we have mentioned the thermodynamical approaches (accounting for screening of Coulomb repulsion) which were developed by Jancovici and further developed by Ichimaru [60, 61].

We will now present a different approach on the basis of Gamov's microscopic theory and the theory of microfields. Gamov's formula for the rate of two-body fusion even if has been obtained by solution of the Schrödinger equation for nonrelativistic inelastic scattering exactly coincides (in the exponential part) with the quasiclassical formula for particle penetration through a potential barrier. Thus, it is possible to avoid the complicated solution of the Schrödinger equation, by using instead the quasiclassical formula. Quasiclassically the penetration probability W through the barrier is expressed by well known dependence

$$W = \exp\left(-(2/\pi)\int_a^b p\ \mathrm{d}r\right). \tag{23}$$

Here a and b are the classical turning points. In our case $a = r_{\mathrm{n}}$ is the nuclear radius, and $b = r_{\mathrm{b}}$ is the radius of the barrier.

On the basis of this formula we can account for the influence of surrounding particles in a rather natural way. Indeed, the fluctuations of the particle positions in the plasma (due to the thermal motion) lead to fluctuations of the microscopic electric field at each point of the plasma, according to Holtsmark's classical work on ideal plasmas. The nonideality of the plasma leads to quantitative corrections to Holtsmark's result [62] but there are no qualitative changes: the value of the root mean square amplitude of this random field remains large, and is about the strength of the Coulomb field of a unit charge particle at the characteristic interparticle distance d_{i} [62]. Thus under each act of nuclear fusion the value of the Coulomb barrier is strongly influenced by the random field potential. This correction can be accounted for by introducing into the momentum of the reacting particle the value of the random field potential.

Because all particles in the plasma participate in the thermal motion, the random microscopic field will have a complicated spectrum. According to Baranger [62], we note two parts of this field: low-frequency contributions (due to the dynamics of the ions), and high-frequency contributions (mainly due to the motion of the electrons). It is easy to see that the time changes of the field should be much slower than the time of fusion, i.e. the time for one particle to penetrate through the potential barrier of another particle. If the high-frequency component provides such rapid changes during the fusion time then it is possible to suppose that this component does not yield a correction for the barrier potential (because it is totally averaged over fusion times). There is just one exception, namely the hypothetical process of cold fusion, when this component has a stationary character. Indeed, the low-frequency component contributes to this correction because the changes of the random field due to the motion of ions are slow enough.

Now, we will calculate the probability of barrier penetration in the quasiclassical approximation taking into account the low-frequency component of the random microscopical field. The momentum p is defined by

$$p = \left((2m)[(Z^2e^2/r) - \epsilon - ZFer]\right)^{1/2}. \tag{24}$$

Here ϵ is the projectile energy, m is the (reduced) mass of projectiles and Z is the ion charge (we suppose that our plasma contains just one type of ion), r denotes the distance between the reacting nuclei and F is the field strength. We suppose that $a = 0$ (the finite size of nuclei can be easily evaluated if necessary), and introduce the parameter

$$\zeta = 4Z^3e^3F/\epsilon^2. \tag{25}$$

Then, expression (23) can be rewritten as

$$W(F,\epsilon) = \exp\left(-\frac{2(2m\epsilon^3)^{1/2}}{\hbar ZeF}\int_0^d \frac{\mathrm{d}x((d-x)(x-c))^{1/2}}{x^{1/2}}\right) \tag{26}$$

where

$$d = (1+\zeta)^{1/2} - 1 \qquad c = -(1+\zeta)^{1/2} - 1. \tag{27}$$

The integral in the expression for W can be evaluated through complete elliptical integrals of the first kind $K(k)$ and of the second kind $E(k)$. Here the argument k is defined by

$$k = \left(\frac{d}{(d-c)}\right)^{1/2} \tag{28}$$

$$W(F,\epsilon) = \exp\left(\frac{2((d-c)m\epsilon^3)^{1/2}[cK(k)-2E(k)]}{3\hbar ZeF}\right). \tag{29}$$

The mean reaction rates are obtained by averaging over the thermal energies ϵ and the random fields F. In the case of the absence of electric fields we get Gamov's result. By averaging over the thermal distribution of ϵ, we obtain Thompson's result [63].

If ζ is small but not equal to zero, we can expand our general formula (29) under the exponent into a Taylor series. Keeping just the first term with respect to ζ we find

$$W(F,\epsilon) = \exp(-\pi(2m/\epsilon)^{1/2}(Z^2e^2/\hbar)(1-\zeta/96)). \tag{30}$$

The factor

$$A^* = \exp(\pi(2m/\epsilon)^{1/2}(Z^2e^2\zeta/96\hbar)) \tag{31}$$

can be interpreted as the relative enhancement of the fusion rate by the suppression of the Coulomb barrier by a random (low-frequency) field. However, the validity of this formula is restricted to the case when the action of this field is small. For example, for the deuterium–tritium reaction under liquid fuel density and a temperature of 5 keV the value of A^* is about 10^{-6}. The case $\zeta \simeq 1$ for hydrogen plasmas corresponds to the value of $F \simeq 0.5\times10^{10}$ CGS. Such fields can be obtained in plasmas at densities of reacting particles of about $n \simeq 10^{30}$ cm^{-3}, which is slightly less then the densities inside white dwarfs [61].

Let us now consider another case when ζ is rather large ($\zeta \to \infty$). This case is also of interest for reactions in white dwarfs. Under the condition

$$\zeta \to \infty \qquad k \to \sqrt{2}/2 \tag{32}$$

we get finally

$$W = \exp\left(-\frac{8\pi K(1/\sqrt{2})}{3\hbar}\left(\frac{Z^5m^2e^5}{F}\right)^{1/4}\right). \tag{33}$$

In this case W grows slowly with the field strength F. Practically, we observe a factor $0.9(Z^3e^3F)^{1/4}$ instead of $\sqrt{\epsilon}$ in the formula for small ζ values. We note further that the condition $\zeta \gg 1$ practically corresponds to the nonideal plasma conditions. In order to show this, we take F at the Holtsmark maximum, $\zeta \simeq 6\Gamma^2$, where Γ is the parameter of plasma nonideality. Further, we can determine the relative enhancement of the fusion rate in the case of large ζ by dividing the value of $W(F,\epsilon)$ by $W(F=0,\epsilon)$:

$$A^{**} = \exp\left(\frac{\pi(2m)^{1/2}Z^2e^2}{\hbar\epsilon^{1/2}} - \frac{8\pi K(2^{1/2}/2)}{3\hbar}\left(\frac{Z^5m^2e^5}{F}\right)^{1/4}\right). \tag{34}$$

Let us now estimate the enhancement factors for several examples. As a first approximation we replace the field strength F by the maximal value of the low-frequency ionic field, which is according to Holtsmark's distribution [62]

$$F_{\max} \simeq 3.9en^{2/3}. \tag{35}$$

We now consider the field influence for the proton–proton fusion in the interior of the Sun. Here the density is $n = 3.3\times10^{25}$ cm^{-3}, the plasma temperature is about $T \simeq 1.3$ keV [61]. Introducing the maximal low-frequency ionic field, for such conditions we get $\zeta \ll 1$, and using (31) we find $A^* = \exp(0.0011)$. According to this estimate the enhancement is about 0.11%, i.e. even smaller than the 2% obtained by Ichimaru [61].

For white dwarfs (WD), let us estimate the enhancement for the carbon–carbon reaction [61]. Here the density is $n \simeq 10^{32}$ cm^{-3}, and the temperature is $T \simeq 4.5$ keV, and therefore $\zeta \gg 1$. By using Holtsmark's maximum for F, which yields the estimate $3.9en^{2/3}$, the total enhancement can be obtained from (34). We find $\ln A^{**} = 41.1$ (to be compared with the enhancement factor $\ln A^{**} = 23.5$ given by Ichimaru [61]). For He–He reactions in white dwarfs we get $n = 1.47 \times 10^{31}$ cm^{-3} and $T \simeq 0.9$ keV, $\zeta \gg 1$, $\ln A^{**} = 22$.

Finally, let us consider ICF plasmas. For plasmas compressed 350 times by laser driving (e.g. by an ICF process for the deuterium–tritium reaction) the characteristic densities are $n = 0.7 \times 10^{25}$ cm^{-3} and the plasma temperature $T \simeq 4.5$ keV. Under such conditions we find with $F = 3en^{2/3}$, $\zeta \ll 1$, and, using (31) $A^* = \exp(0.000\,22)$, i.e. the enhancement is about 0.022% (to be compared with 0.4% obtained by Ichimaru [61]). Summarizing we may state that the estimated enhancement factor obtained from our microfield approach is in general rather small (even smaller than the values estimated by Ichimaru). It remains, however, to solve the problem of a more correct account for the nonideality effects in the microfields.

4. Conclusions

We have demonstrated that a large part of the universe is in a dense plasma state. Under laboratory conditions plasma nonideality requires rather exotic conditions, in particular a very high energy density. Nevertheless, several rather interesting phenomena such as arcs belong to this class. As we have shown, nonideality effects influence thermodynamic, transport and kinetic properties. Of special importance is the influence of nonideality on chemical equilibria and on reaction rates. The influence on fusion rates is in general rather weak, except under the conditions of astrophysical objects.

In spite of the fact that plasma nonideality will not be a central theme of fusion research we would like to express the hope that the theoretical analysis of nonideality effects and the experimental expertise developed by researchers in this field will contribute to the solution of special interesting problems.

Acknowledgments

The authors thank D Beule, M Kasch, Yu L Klimontovich, W D Kraeft, D Kremp, V Yu Podlipchuk, R Redmer, G Röpke and M Schlanges for many fruitful discussions and a collaboration on special topics of the problems discussed here.

References

[1] Ebeling W, Kraeft W D and Kremp D 1976 *Theory of Bound States and Ionization Equilibrium in Plasmas and Solids* (Berlin: Akademie); 1979 Extended Russian translation (Moscow: Mir)

[2] Ebeling W, Förster A, Fortov V E, Gryaznov V K and Polishchuk A Ya 1991 *Thermophysical Properties of Hot Dense Plasmas* (Stuttgart and Leipzig: Teubner)

[3] Van Horn H M and Ichimaru S (eds) 1993 *Strongly Coupled Plasma Physics* (Rochester: Rochester University Press)

[4] Kraeft W D and Schlanges M (eds) 1996 *Physics of Strongly Coupled Plasmas* (Singapore: World Scientific)

[5] Eliezer S, Ghatak A and Hora H 1986 *An Introduction to Equations of State: Theory and Applications* (Cambridge: Cambridge University Press)

[6] March N H and Tosi M P 1984 *Coulomb Liquids* (London: Academic)

[7] Ebeling W 1967 *Ann. Phys.* **19** 104; 1968 *Ann. Phys.* **21** 315; 1969 *Ann. Phys.* **22** 33, 383, 392; 1968 *Physica* **38** 378; 1968 **40** 290; 1969 **43** 293; 1974 **73** 573

[8] Rohde K, Kelbg G and Ebeling W 1968 *Ann. Phys.* **22** 1; **21** 235;
Kraeft W and Kremp D 1968 *Ann. Phys.* **20** 340

[9] Eschrig K 1996 *The Fundamentals of Density Functional Theory* (Stuttgart and Leipzig: Teubner)

[10] Ebeling W, Kraeft W D and Kremp D 1970 *Beitr. Plasmaphys.* **10** 237

[11] Kraeft W D, Kremp D, Ebeling W and Röpke R 1986 *Quantum Statistics of Charged Particle Systems* (Berlin: Academic); 1986 (New York: Plenum); 1988 Russian Translation (Moscow: Mir)

[12] Ichimaru S 1992 *Statistical Plasma Physics: I. Basic Principles* (Reading, MA: Addison-Wesley); 1994 *Statistical Plasma Physics: II. Condensed Plasmas* (Reading, MA: Addison-Wesley)
[13] Ichimaru S and Ogata S (eds) 1995 *Elementary Processes in Dense Plasmas* (Reading, MA: Addison-Wesley)
[14] Ebeling W and Förster A 1995 *Elementary Processes in Dense Plasmas* (Reading, MA: Addison-Wesley) p 165
[15] Alastuey A and Martin Ph A 1989 *Phys. Rev.* A **40** 6485
Alastuey A and Perez A 1992 *Europhys. Lett.* **20** 19
Alastuey A, Cornu F and Perez A 1994 *Phys. Rev.* E **49** 1077; 1995 *Phys. Rev.* E **51** 1725
[16] Ebeling W 1990 *Contrib. Plasma Phys.* **30** 553; 1993 **33** 492
[17] Zamalin V M, Norman G E and Filinov V S 1977 *The Monte Carlo Method in Statistical Mechanics* (Moscow: Nauka) (in Russian)
[18] Pierleoni C, Ceperley D M, Bernu B and Margo W R 1994 *Phys. Rev. Lett.* **73** 2145
[19] Klakow D, Toepffer C and Reinhard P-G 1994 *Phys. Lett.* **192A** 55; 1994 *J. Chem. Phys.* **101** 10 766
[20] Ebeling W, Förster A and Podlipchuk V 1996 *Phys. Lett.* **218A** 297
[21] Riemann J, Schlanges M, De Witt H E and Kraeft W D 1995 *Physica* **219A** 423
[22] Lehmann H and Ebeling W 1996 *Phys. Rev.* E at press
[23] Ebeling W, Förster A and Radtke R (eds) 1992 *Physics of Nonideal Plasmas* (Stuttgart and Leipzig: Teubner)
[24] Förster A, Kahlbaum T and Ebeling W 1991 *High Press. Res.* **7** 375; 1992 *Laser Part. Beams* **10** 253
[25] Ebeling W, Förster A., Richert W and Hess H 1988 *Physica* **150A** 159
[26] Förster A and Ebeling W 1992 *Physics of Nonideal Plasmas* (Reading, MA: Addison-Wesley) p 95; 1993 *Strongly Coupled Plasma Physics* (Reading, MA: Addison-Wesley) p 147
[27] Beule D, Ebeling W, Förster A and Kasch M 1996 *Physics of Strongly Coupled Plasmas* (Reading, MA: Addison-Wesley) p 49
[28] Christenssen-Dalsgaard J and Däppen W 1992 *Astron. Astrophys. Rev.* **4** 267
[29] Fortov V E and Iakubov I T 1984 *Physics of Nonideal Plasma* USSR Academy of Sciences, Chernogolovka (in Russian); 1990 English Translation (New York: Hemisphere); 1994 *Nonideal Plasmas* (Moscow: Energoatomizdat)
[30] Beule D, Ebeling W and Förster A 1996 *Physica* A submitted
[31] Redmer R and Röpke G 1985 *Physica* **130A** 523; 1989 *Contrib. Plasma Phys.* **29** 343
Reinholz H, Redmer R and Nagel St 1995 *Phys. Rev.* E **52** 5368
[32] Landau L D and Zeldovich Ya B 1943 *Acta Physico-Chem. URSS* **18** 194
[33] Norman G and Starostin A 1968 *Teplophys. Vys. Temp.* **6** 410; 1970 *Teplophys. Vys. Temp.* **8** 413
[34] Ebeling W and Sändig R 1973 *Ann. Phys* **28** 289
[35] Ebeling W and Richert W 1985 *Phys. Lett.* **108A** 80
[36] Saumon D and Chabrier G 1989 *Phys. Rev. Lett.* **62** 2397
[37] Mott F 1968 *Rev. Mod. Phys.* **40** 677
[38] Marley M S and Hubbard W B 1988 *Icarus* **73** 536
[39] Hensel F 1990 *J. Phys.: Condens. Matter* **2** SA33
[40] Franz G 1980 *Doctoral Thesis* University of Marburg
[41] Young D A 1991 *Phase Diagrams of the Elements* (Berkeley, CA: University of California Press)
[42] Likalter A 1985 *Teplofiz. Vys. Temp.* **23** 465; 1992 *Sov. Phys.–Usp.* **35** 591
[43] Hess H 1995 *Phys. Chem. Liq.* **30** 251
Hess H and Schneidenbach H 1996 *Z. Metallkd.* accepted
[44] Hoshino H, Schmutzler R W, Warren W W and Hensel F 1976 *Phil. Mag.* **33** 255
Hoshino H, Schmutzler R W and Hensel F 1976 *Ber. Bunsenges. Phys. Chem.* **80** 27
[45] DeSilva A W and Kunze H J 1994 *Phys. Rev.* E **49** 4448
[46] Ben-Yosef N and Rubin A G 1969 *Phys. Rev. Lett.* **23** 289
[47] Drawin H W and Felenbok P 1965 *Data for Plasmas in Local Thermodynamic Equilibrium* (Paris: Gauthier-Villars)
[48] Griem H 1968 *Plasma Spectroscopy* (New York: McGraw-Hill)
[49] Kobzev G A, Iakubov I T, Popovich M M (eds) 1995 *Transport and Optical Properties of Nonideal Plasma* (New York: Plenum)
[50] Ross M, Ree F H and Young D A 1983 *J. Chem. Phys.* **79** 1487
Nellis W J *et al* 1983 *J. Chem. Phys.* **79** 1480; 1984 *Phys. Rev. Lett.* **53** 1248
[51] Weir S T, Mitchell A C and Nellis W J 1996 *Phys. Rev. Lett.* **76** 1860
[52] Goncharov A F, Mazin I I, Eggert J H, Hemley R J and Mao H K 1995 *Phys. Rev. Lett.* **75** 2514
[53] Klimontovich Yu L 1982 *Kinetic Theory of Electromagnetic Process* (Heidelberg: Springer)

[54] Biberman L M, Vorob'ev V S and Iakubov I T 1987 *Kinetics of Nonequilibrium Low-Temperature Plasmas* (New York: Plenum)
[55] Drawin H W and Emard F 1977 *Physica* **85C** 333
[56] Ebeling W, Förster A, Kremp D and Schlanges M 1989 *Physica* **159A** 285
[57] Schlanges M, Bornath Th and Kremp D 1988 *Phys. Rev.* A **48** 2174
[58] Beule D, Conrad, Ebeling W and Förster A 1995 *INP-Report IX (Greifswald)*
[59] Ebeling W and Leike I 1991 *Physica* **170A** 682
[60] Jancovici B 1977 *J. Stat. Phys.* **17** 357
[61] Ichimaru S 1993 *Rev. Mod. Phys.* **65** 255
[62] Baranger M and Mozer B 1959 *Phys. Rev.* **115** 521; 1960 *Phys. Rev.* **118** 626
[63] Thompson W B 1957 *Proc. Phys. Soc.* B **70** 1